Polyoxymethylene/Polyurethane/Alumina Ternary Composites: Structure, Mechanical, Thermal and Dielectric Properties

S. Siengchin,[1] J. Karger-Kocsis,[1] G. C. Psarras,[2] R. Thomann[3]

[1]*Institute for Composite Materials (Institut für Verbundwerkstoffe GmbH), Kaiserslautern University of Technology, D-67663 Kaiserslautern, Germany*
[2]*Department of Materials Science, School of Natural Sciences, University of Patras, GR-26504 Patras, Greece*
[3]*Institut für Makromolekulare Chemie und Freiburger Materialforschungszentrum, Albert-Ludwigs-Universität Freiburg, D-79104 Freiburg, Germany*

Received 3 December 2007; accepted 24 April 2008
DOI 10.1002/app.28589
Published online 25 July 2008 in Wiley InterScience (www.interscience.wiley.com).

ABSTRACT: Ternary composites composed of polyoxymethylene (POM), polyurethane (PU), and boehmite alumina were produced by melt blending with and without latex precompounding. Latex precompounding served for the predispersion of the alumina particles. The related masterbatch (MB) was produced by mixing the PU latex with water-dispersible boehmite alumina. The dispersion of the alumina was studied by transmission and scanning electron microscopy techniques (TEM and SEM, respectively) and discussed. The crystallization of POM was inspected by means of differential scanning calorimetry (DSC) and polarized optical microscopy (DSC and polarized light microscopy, respectively). The mechanical and thermomechanical properties of the composites were determined in uniaxial tensile, dynamic-mechanical thermal analysis (DMTA), short-time creep tests (performed at various temperatures), and thermogravimetric analysis (TGA). The melt flow of the composites was characterized in a plate/plate rheometer. In addition, the dielectric response of the nanocomposites was investigated by means of broadband dielectric spectroscopy at an ambient temperature. The composites produced by the MB technique outperformed the direct melt (DM) compounded composites in respect to the thermal and mechanical characteristics. © 2008 Wiley Periodicals, Inc. J Appl Polym Sci 110: 1613–1623, 2008

Key words: polyoxymethylene; impact modifier; polyurethane; alumina; composites; structure-property relationships

INTRODUCTION

Research on polyoxymethylene (POM) became under spot of interest due to its excellent mechanical properties (creep resistance, high tensile strength, stiffness, and heat deflection temperature) and resistance against various solvents.[1–3] The extreme high crystallinity of POM, accompanied with brittleness, and the low thermooxidative stability are the limiting factors of its applications.[4,5] Blending with thermoplastic polyurethane (TPU) elastomer,[6–9] or compounding with both rubber and rigid particles[10] has attracted considerable attention in the recent years due to the achieved improvements in toughness characteristics of POM.

To prepare polymeric nanocomposites, various methods have been followed such as *in situ* polymerization, melt blending, and solution/dispersion techniques.[11,12] Note that, in the corresponding nanocomposites, the fillers are dispersed in nanoscale. It was recognized earlier that the preparation technique of the nanocomposites has a strong impact on the dispersion of the nanoparticles.[12] We have demonstrated that polystyrene (PS)-based nanocomposites can be produced using water-dispersible alumina, as filler, by adopting the latex compounding/latex coagulation method.[13] In that case, the alumina became nanoscale dispersed in the PS latex. It was shown that direct melt (DM) mixing of the alumina with PS resulted in microcomposites, whereas the masterbatch (MB) technique (latex route) resulted in nanocomposites. This allowed us to conclude the effects delivered by the nanoscale dispersion. Recently, nanosilica/POM latex combination was used by Wang et al.[14] to obtain a hybrid film, which exhibited good surface properties and better thermal behavior than the unmodified POM. Recall that the POM is prone for thermal decomposition and thus the improvement of its thermal resistance is of great practical relevance.

Usually, toughening of thermoplastics is associated with a reduction in stiffness, strength, and thermal resistance. This rule of thumb may not hold for

Correspondence to: J. Karger-Kocsis (karger@pt.bme.hu).

© 2008 Wiley Periodicals, Inc.

TABLE I
Recipes and Designations of the POM-Based Systems

		Masterbatch technique (MB)	Direct melt mixing (DM)
Sample designation	PU content (wt %)	11N7-80 alumina content (wt %)	11N7-80 alumina content (wt %)
POM	–	–	–
POM/PU (10)	10	–	–
POM/PU (10)/11N7-80 (3)	10	3	–
POM/PU (10)/11N7-80 (3)	10	–	3

nanocomposites for which simultaneous improvements in the above properties were also reported (Ref. 11 and references therein).

This work addresses the toughening and reinforcement of POM via a novel method, which allow us to achieve micro and nanocomposites. As toughening agent for POM TPU was selected, polyurethane (PU) in latex form has been chosen due to the following reasons. Boehmite alumina is water dispersible, and thus its nanoscale dispersion can likely be achieved also in aqueous PU latex. Moreover, using latex (water)-mediation, no coupling agent is required to reach the required fine dispersion of the alumina. It is also noteworthy that the mean particle size of rubber latices is closely matched with that one required from usual toughening agents, impact modifiers. This fact may be highly beneficial for online extrusion compounding processes whereby PU latex is injected in the POM melt (being in progress in our laboratory).

Through the PU latex, working as "carrier" for the alumina in this case, a much finer dispersion than by DM compounding (when adding alumina in dry powder form) can be expected. Our working hypothesis was that the fine (nanoscale) dispersion of the alumina filler may yield additional improvements in the mechanical and thermal properties of POM/PU binary blends compared to those containing coarser alumina dispersions (microscale). So, the goal of this study was to explore the potential of the latex-mediation technique to disperse boehmite alumina in nanoscale. Further aims of this work were to produce POM/PU/alumina ternary systems by melt mixing with and without a PU/alumina MB (received by latex compounding) and to compare the structure-property relationships of the resulting nano and microcomposites.

EXPERIMENTAL

Materials and preparation of composites

Water-dispersible boehmite alumina [AlO(OH); Dispal® 11N7-80 of Sasol GmbH, Hamburg, Germany] served as filler. Its characteristics are as follows: Al_2O_3 content, 80 wt %; specific surface area, 100 m^2/g; mean dispersed particle size in water, 220 nm. Latex of thermoplastic PU with 50 wt % dry content (Acralen U 550) was kindly supplied by Polymer Latex GmbH (Marl, Germany). Granulated POM (Hostaform C 9021, Ticona GmbH, Frankfurt, Germany) was used as polymeric matrix for all composite systems. Its volumetric melt flow rate (MVR at 190°C/2.16 kg) was 8 cm^3/10 min.

The POM/PU/alumina ternary systems were prepared by two methods: (a) DM compounding and (b) melt compounding using a MB containing both PU and alumina (MB technique). The alumina content in the corresponding composites was set for 3 wt %. Melt mixing occurred in laboratory kneader (Type 50 of Brabender, Duisburg, Germany) at T = 190°C and rotor speed of 60 rpm. The alumina powder (DM) or alumina-containing PU (MB) was introduced in the POM system after melt mastication of the latter for 2 min. The duration of the melt mixing for both DM and MB was 6 min. POM/PU binary composites were also produced by DM mixing by incorporating dried PU. The composition and designation of the compounds studied are given in Table I.

A scheme of the MB technique is given in Figure 1. The MB was produced as described below. First, an aqueous alumina slurry (10 wt %) was prepared at ambient temperature through mechanical stirring for 30 min. Then the PU latex was introduced in this slurry and stirred for further 30 min. The resulting slurry was poured in a framed glass plate and dried for 5 days at room temperature (RT). This resulted in a PU film as the glass transition temperature (T_g) of PU is much lower than RT. The compounds, after melt mixing in the Brabender kneader, were compression molded into 1-mm thick sheets at T = 200°C using a hot press (EP-Stanzteil, Wallenhorst, Germany). Although this technique is not straightforward for POM, the press conditions did not result in prominent thermal degradation of POM. This claim is based on inspection of the fracture surfaces of the specimens where no formaldehyde-caused bubbles were seen. The composites of POM/PU/alumina systems are listed in Table I.

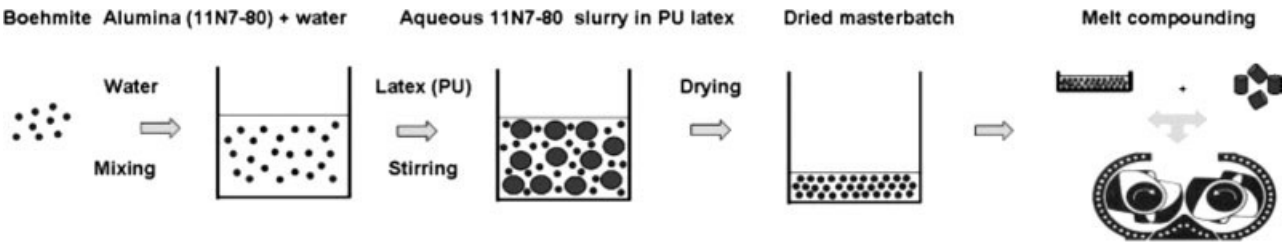

Figure 1 Scheme of the preparation of POM/PU/alumina composites via the masterbatch method.

Characterization and testing

Morphology detection

The dispersion of alumina in the POM nanocomposites was studied by transmission and scanning electron microscopy techniques (TEM and SEM, respectively). TEM measurements were carried out with a Zeiss LEO 912 Omega transmission electron microscopic (Oberkochen, Germany) applying an acceleration voltage of 120 kV. Thin sections ($\sim$ 50 nm) were cut at RT with a Diatome diamond knife (Hatfield, PA) using an Ultracut E microtome (Reichert and Jung, Vienna, Austria).

The fracture surfaces of tensile-loaded specimens were subjected to SEM inspection in a high magnitude Supra^{TM} 40VP SEM (Carl Zeiss GmbH, Oberkochen, Germany). The surface was carbon-coated prior to SEM inspection performed at low acceleration voltage.

Crystallization and melting properties

The spherulite growth was observed by polarized light microscopy (PLM). Samples were isothermally crystallized in a hot stage (THMS 600/S, Raczek Analysentechnik, Wedemark, Germany). Thin films with a thickness of 20–30 μm were used. The film was melted at 200°C for 1 min and then cooled to the isothermal crystallization temperature (T = 148°C) where it was hold for 60 min.

Differential scanning calorimetry (DSC) traces were recorded on a Mettler DSC 821 device in the temperature range from −100 to 200°C at a heating and cooling rate of 10°C/min. The crystallinity (X_c) of POM was calculated from the following equation:

$$X_c = \frac{\Delta H_m}{\left(\Delta H_m^0\right)} \times 100\% \quad (1)$$

where ΔH_m is the melt enthalpy of the POM in the sample (i.e., net POM content considered) and ΔH_m^0 is the theoretical enthalpy of POM for X_c = 100% (186 J/g), as reported in Ref. 10.

Thermal and thermomechanical properties

Thermogravimetric analysis (TGA) was performed on a TG50 Mettler Toledo device (Giessen, Germany). TGA experiments were conducted in the temperature range from 25 to 600°C under oxygen at a heating rate of 10°C/min.

Dynamic mechanical analysis (DMA) was made in tensile mode at 1 Hz frequency using a DMA Q800 apparatus (TA Instruments, New Castle, NJ). The storage and loss moduli (E', E'') along with mechanical loss factor (tan δ) were determined as a function of the temperature (T = −100°C ... +150°C). The strain applied was 0.1%, and the heating rate was set for 3°C/min. The specimen was a dumbbell-shaped type (S3A according to DIN 53504).

Mechanical response

Short-time creep tests were made in tensile mode at different temperatures using the above DMA apparatus. The creep and recoverable compliance were determined as a function of the time (t_{creep} = 60 min and $t_{recovery}$ = 120 min) at T = 30°C. The applied tensile stress was 6 MPa (at 0.35% strain). This was derived from a test series checking the presence of linear isochronous deformation. Creep test was performed on dumbbell-shaped specimens (5B type according to DIN-EN ISO 527) by considering their rectangular section.

The temperature dependence of the creep response of the POM and its composites were studied in the range from −50 to 80°C. Isothermal tests were run on the same specimen, under 6 MPa load, in the above temperature range. The temperature was increased stepwise by 5°C and the specimen equilibrated at each temperature for 5 min. During the isothermal tests, the duration of the creep testing was, however, only 15 min.

Tensile tests were performed on dumbbell-shaped specimens (S3A according to DIN 53504) on a Zwick 1474 (Ulm, Germany) universal testing machine. Tests were run at RT at v = 2 mm/min crosshead speed, and the related mean strength and elongation at break values were determined.

Dielectric response

Broadband dielectric measurements were performed in the frequency range of 10^{-3}–10^{7} Hz, by means of

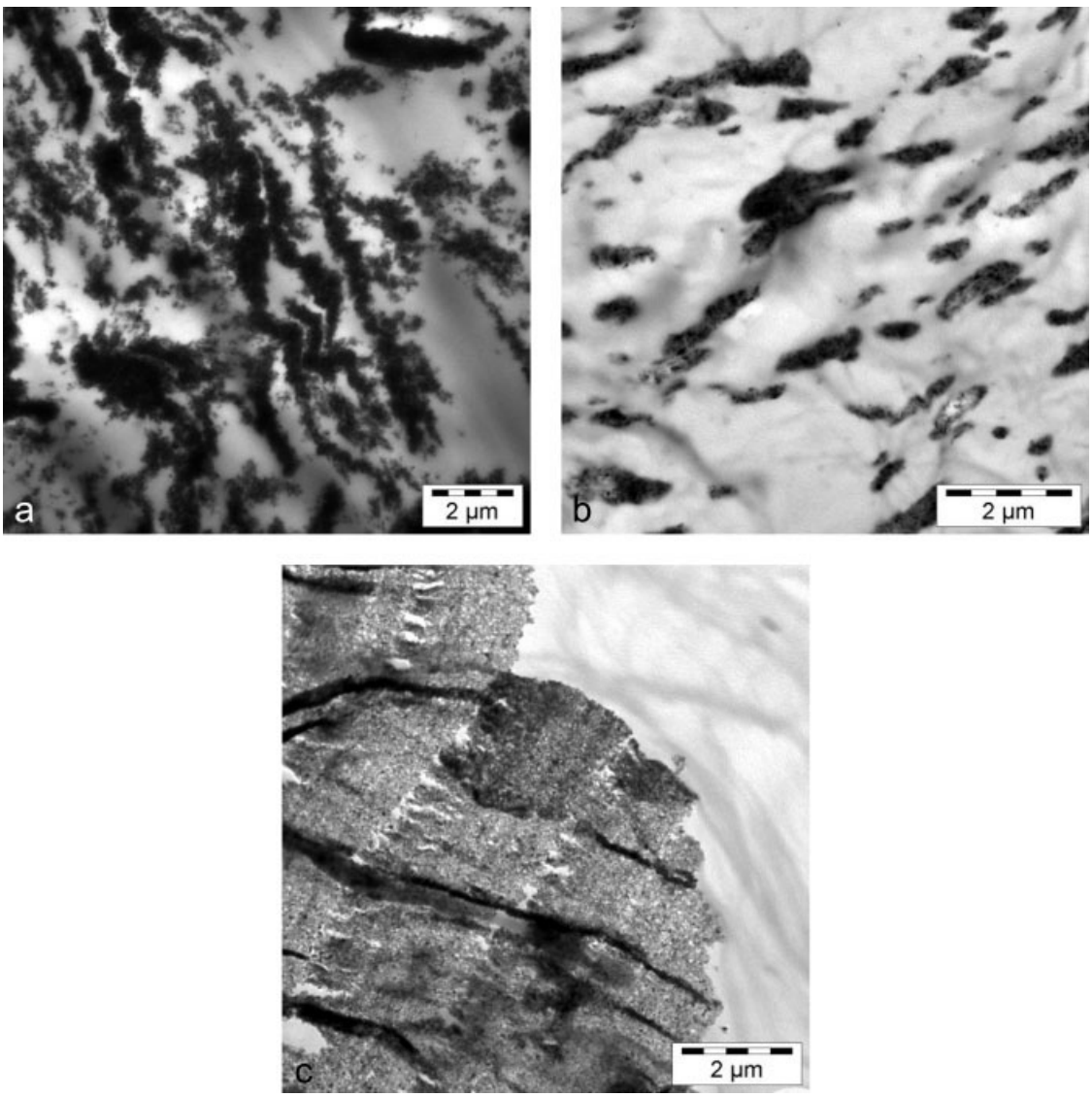

Figure 2 TEM pictures taken from (a) PU/alumina (MB), (b) the composites produced by masterbatch technique, and (c) direct melt compounding.

α-N Frequency Analyzer, supplied by Novocontrol Technologies GmbH (Hundsangen, Germany) at RT. The amplitude of the test voltage was kept constant at 100 mV. The employed test cell was a two-electrode gold-coated plate capacitor, BDS 1200, supplied also by Novocontrol, which was suitably shielded.

Rheology

A controlled strain rheometer (ARES of Rheometric Scientific, NJ) was used in parallel plate configuration (diameter of the plate: 25 mm) to measure the melt rheology of the POM and its composites at $T = 190^{\circ}C$. Oscillatory shear measurements were performed on each sample by setting the strain amplitude for 1%. This was derived from a strain sweep test series checking the presence of the linear viscoelastic region. The gap between the plates was 2 mm.

RESULTS AND DISCUSSION

Morphology detection

TEM picture taken from the dried PU/alumina MB (alumina content: 30 wt %) is shown in Figure 2(a). When this PU/alumina (MB) is melt mixed with the POM granules, a fine alumina dispersion is achieved [cf. Fig. 2(b)]. By contrast, TEM pictures taken from the DM compounded POM/PU/alumina ternary composite evidence the presence of large agglomerates of the alumina particles [cf. Fig. 2(c)]. One can thus state that the alumina particles are nanoscale and microscale dispersed using MB and DM, respectively.

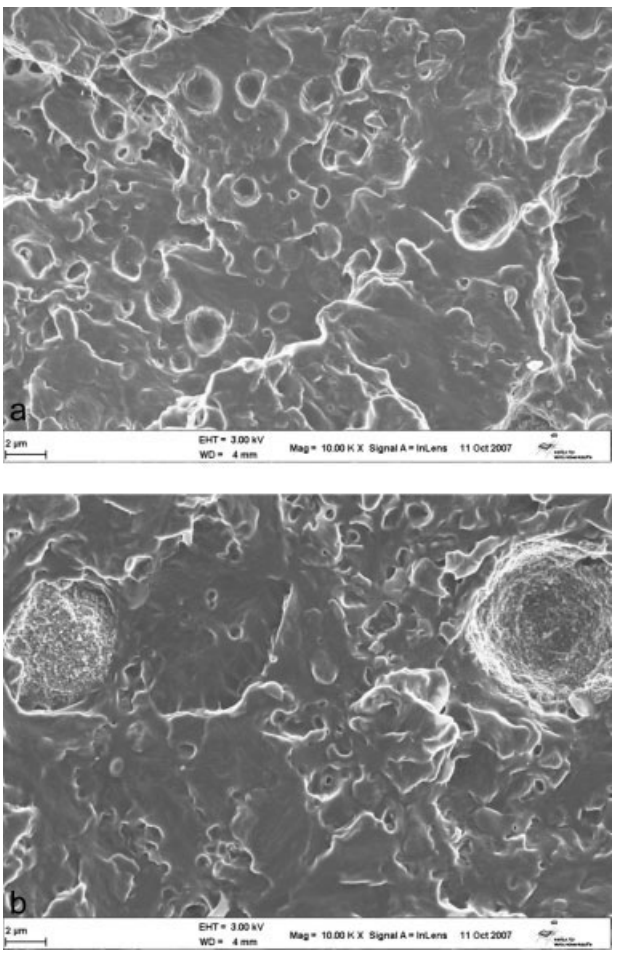

Figure 3 SEM pictures taken from the tensile fracture surfaces of the composites produced by (a) masterbatch technique and (b) direct melt compounding.

Similar observations can be deduced for these ternary systems from SEM micrographs taken from the fracture surfaces (Fig. 3). Alumina agglomerates of several microns can be seen in the POM matrix when produced by DM [cf. Fig. 3(b)]. On the other hand, they must be far better dispersed in the composites produced by the route MB [cf. Fig. 3(a)]. One can also recognize that the PU domains are in the range of 0.5–2.5 μm irrespective of the production method. Recall that this range is markedly larger than the initial size of the PU particles in the corresponding latex.

PLM is an important method to study the morphology of POM.[15,16] Figure 4(a–d) compares the spherulitic structures of POM, POM/PU blend, and POM/PU/alumina ternary composites prepared by MB and DM, respectively. POM crystallizes in large spherulites [cf. Fig. 4(a)]. Addition of PU significantly disturbs the spherulitic structure of POM, however, does not influence much the spherulite size. Some slight reduction in the POM spherulite size in the POM/PU/alumina ternary composites can be observed [cf. Fig. 4(c,d) prepared by MB and DM, respectively] when compared with the neat POM [cf. Fig. 4(a)]. Interestingly, very regular spherulites appear in the ternary composite produced by MB. In line with the SEM results, the large alumina agglomerates are also obvious in the DM composites on the corresponding PLM picture [cf. Fig. 4(d)]. Unlike the spherulite structure, the incorporation of PU and PU/alumina had a marginal effect on the overall crystallinity of POM in the related systems—cf. DSC data summarized in Table II.

Thermomechanical properties

It has been reported that by adding PU[6] and inorganic fillers, such as organoclay,[16] may increase the thermal stability of POM. This is in accordance with our TGA observation (cf. Fig. 5). It can be seen that that the resistance to thermooxidative degradation of the POM/PU blend is slightly lower than that of POM. On the other hand, the POM/PU/alumina ternary composites start to degrade at markedly higher temperature than either POM or POM/PU. There is practically no difference between the TGA traces of the MB and DM composites. Anyway, the incorporation of alumina strongly enhanced the thermooxidative resistance of the POM/PU blend (and a similar effect can be prophesied also for the plain POM).

DMA response

Figure 6(a,b) depicts the storage modulus (E') and mechanical loss factor (tan δ) as a function of temperature for POM, POM/PU blend, and the composites with alumina particles produced by various methods. One can notice that the storage modulus of the composites is enhanced by adding alumina compared to POM/PU blend. Moreover, the E' versus T trace of the DM composite was always below that of the MB version. This can be attributed to the difference in the dispersion stage of alumina as discussed earlier. Figure 6(a) also shows that the highest stiffness exhibited the plain POM in the whole temperature range.

Concerning the relaxation processes, it is well known that pure POM exhibits three transitions.[15,17,18] The relaxation transition (γ) located at around −60°C is assigned to the glass transition temperature [T_g; cf. Fig. 6(b)]. The two peaks, observed at ambient temperature (β-relaxation) and ~ 130°C (α-relaxation), respectively, are usually assigned to the motions of long molecular segments in disordered and well-ordered crystalline phases, respectively.[18] Addition of PU results in a further relaxation, located at about −50°C, representing the T_g of the PU [cf. Fig. 6(b)]. One can notice that the incorporation of PU and alumina increases the intensity of both α and β-relaxations. The most prominent change can be noticed for the β-relaxation. The intensity of this β-peak further increases

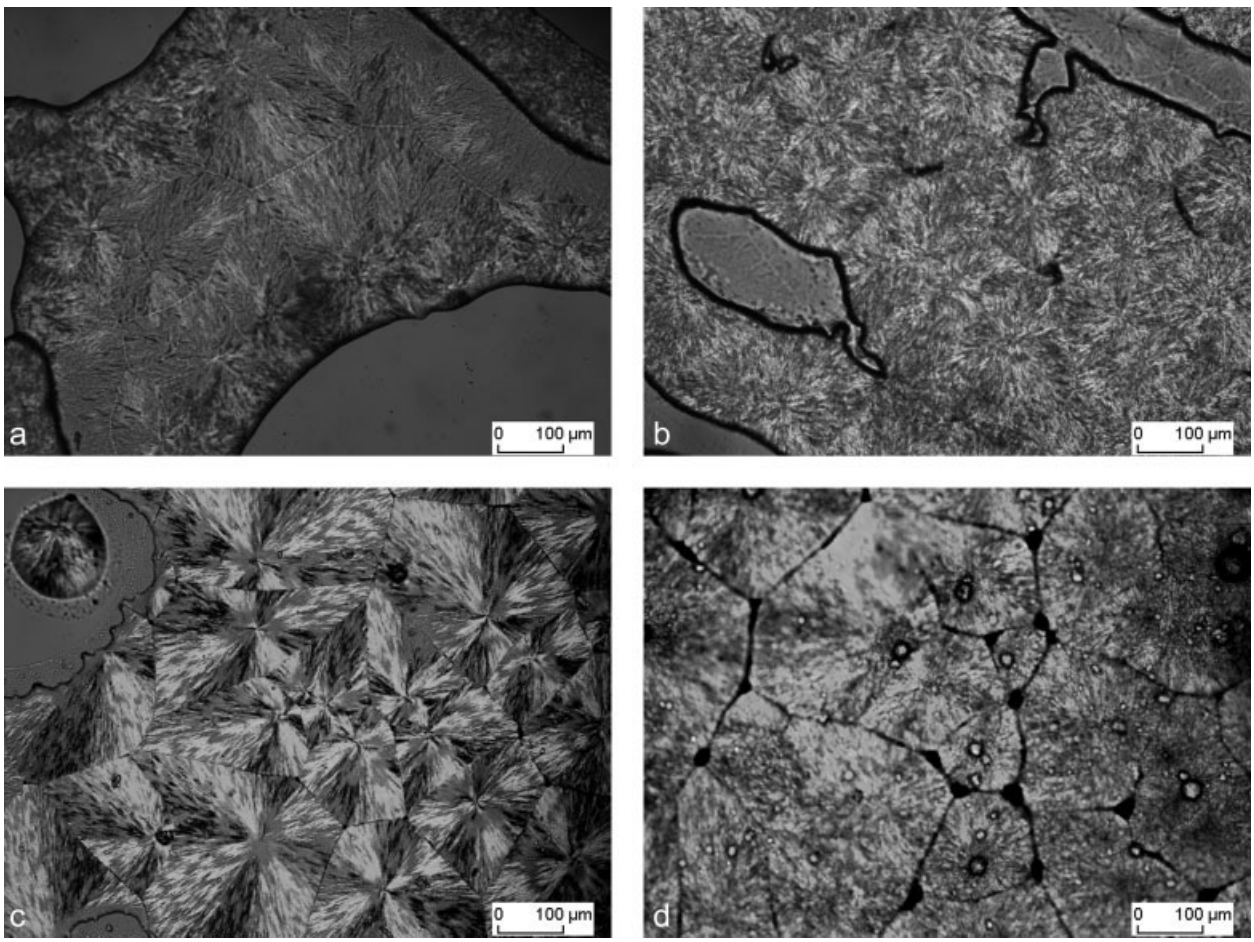

Figure 4 PLM pictures of the isothermally ($T = 148^{\circ}C$) crystallized (a) POM, (b) POM/PU blend, (c) the composites produced by the masterbatch, and (d) direct melt compounding, respectively.

when apart of PU also alumina is present. The related change suggests enhanced segmental motion in the boundary amorphous layers of the crystals in the disordered crystalline phase. The shift of this peak toward higher temperatures due to alumina indicates for the reinforcing effect of the latter [cf. Fig. 6(b)].

Creep behavior

Figures 7 and 8 display the traces of the creep and recovered compliance as a function of time for the POM, POM/PU blend, and the alumina-containing ternary composites produced by DM and MB methods, respectively, at $T = 30^{\circ}C$. The addition of PU into POM matrix resulted in a considerable increase in the creep compliance, as expected owing to this rubber modification (cf. Figs. 7 and 8). The creep compliance values of the composites are smaller compared to the POM/PU blend, showing the reinforcing effect of the alumina. The compliance values were reduced by $\sim$ 23 and 17% compared to the POM/PU blend when alumina was introduced by the MB and DM techniques, respectively.

Figure 9(a–c) demonstrates the effects of increased temperature on the creep response of POM/PU blend and POM/PU/alumina ternary composites

TABLE II
Crystallization and Melting Characteristics for the Systems Studied

Sample designation	T_m (°C)	T_c (°C)	ΔH_m (J/g)	$\%X_c$ (POM)
POM	166.8	145.9	155.2	83.4
POM/PU (10)	168.7	145.9	156.3	84.0
POM/PU (10)/11N7-80 (3) => (DM)	169.3	145.4	158.4	85.2
POM/PU (10)/11N7-80 (3) => (MB)	168.5	146.0	157.1	84.5

T_m, melting temperature; T_c, crystallization temperature; H_m, melting enthalpy; X_c, crystallinity (based on the net POM content).

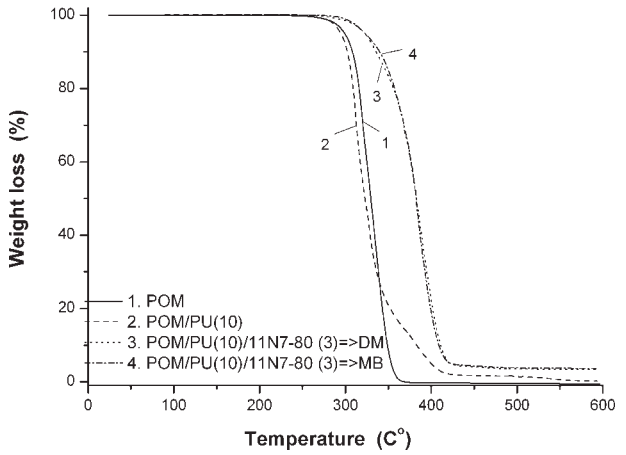

Figure 5 Weight loss versus temperature for the POM and its binary and ternary systems. Designation: MB, masterbatch technique; DM, direct melt compounding.

produced by DM and MB techniques. One can recognize that the creep compliance decreased remarkably with the incorporation of alumina compared to POM/PU blend at all test temperatures.

The creep compliance (D) data, measured in function of both time (t) and temperature ($T = -50 \ldots 80^{\circ}C$), have been "summarized" in creep compliance versus time master curves by adopting the time-temperature superposition (TTS) principle. The creep response at $T_0 = 70^{\circ}C$ was taken for reference. According to the TTS, the creep at other test temperatures than the reference one is linked with the shift factor (a_T) along the time scale (t):

$$D(t, T_1) = \frac{D(t, T_2)}{a_T} \tag{2}$$

Master curves were created by using the related software package of the DMA device used (Rheology Advantage Data Analysis—Version 5.4.8). Note that this software allows us only horizontal shifting of the creep curves along the time axis. The Williams-Landel-Ferry (WLF) equation[19] has been proven for many polymeric materials to fit the creep compliance versus time curves:

$$\log(a_T) = \frac{-C_1 \times (T - T_0)}{C_2 + (T - T_0)} \tag{3}$$

where C_1 and C_2 are constants and T_0 is the reference temperature ($T_0 = 70^{\circ}C$).

Based on eq. (3), one can check whether or not the WLF equation holds for a given system. Figure 10 demonstrates that the course of the a_T values as a function of temperature obeys the WLF equation.

Attempt was also made to check whether the Findley power law model predicts the creep of our systems properly. Note that the related power function is given by (e.g., Refs. 20 and 21)

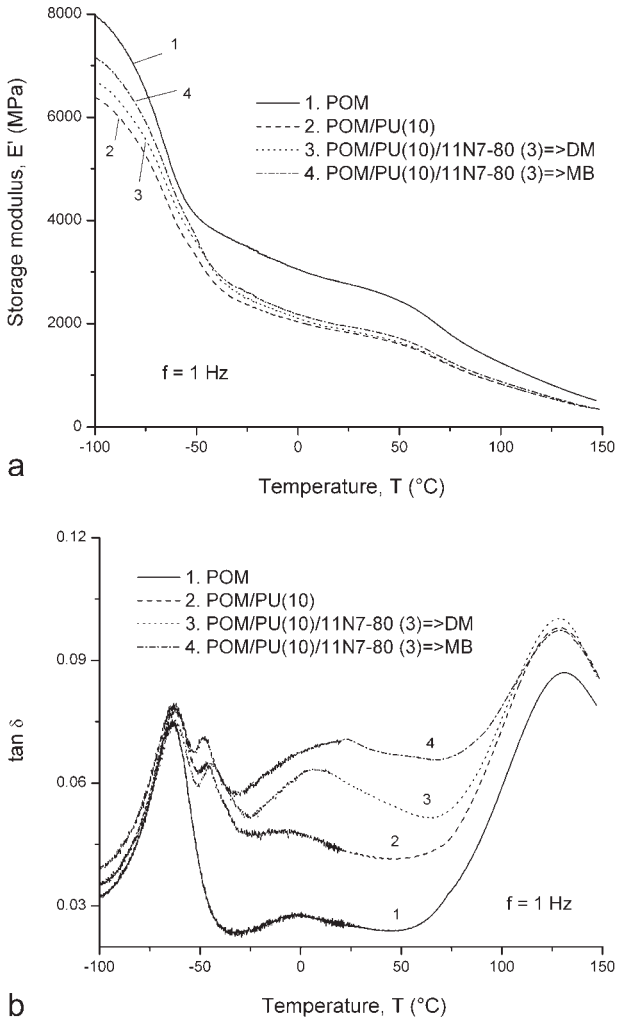

Figure 6 (a) E' versus T and (b) tan δ versus T traces for the POM and its binary and ternary systems studied. For designation, cf. Figure 5.

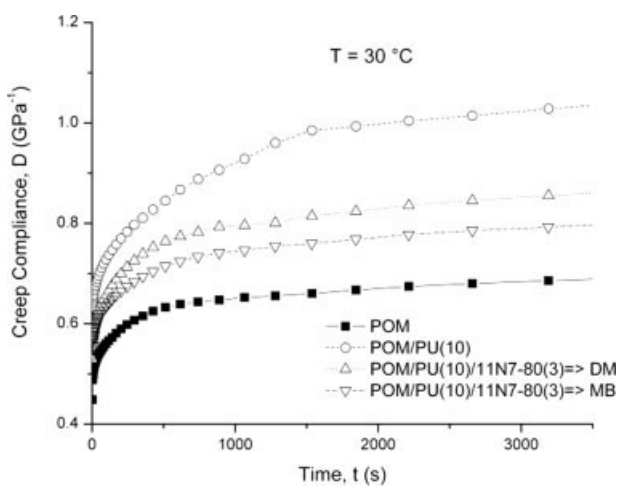

Figure 7 Creep of POM, POM/PU blend, and POM/PU/alumina composites at $T = 30^{\circ}C$. Note: stress applied for t = 60 min. For designation, cf. Figure 5.

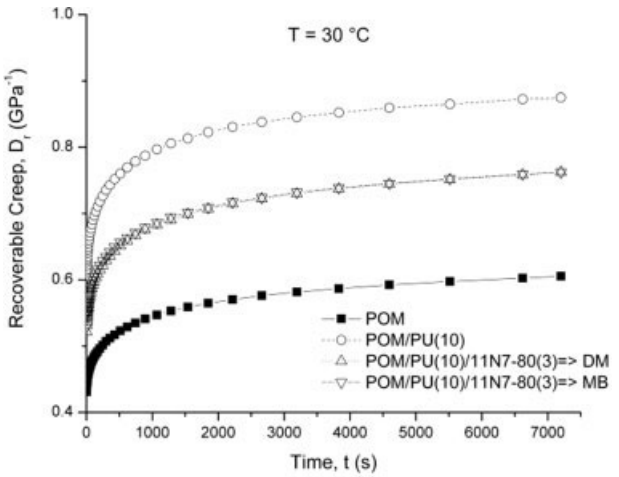

Figure 8 Creep recovery of POM, POM/PU blend, and POM/PU/alumina composites at $T = 30°C$. Note: stress removal for $t = 120$ min. For designation, cf. Figure 5.

$$D_F = D_{F0} + D_{F1} \times t^n \tag{4}$$

where n is a stress-independent constant, D_{F0} is the time-independent compliance, and D_{F1} is the coefficient of the time-dependent compliance term.

Figure 11 shows the constructed master curves along with their Findley fits. The parameters of the Findley power law [cf. eq. (4)] were listed in Table III. Figure 11 shows that the above power law function holds for the POM/PU binary blends and POM/PU/alumina ternary composites produced by different methods. The creep results, when summarized in compliance versus time master curves, proved to be slightly different for the DM and MB composites. The MB produced composite-exhibited better creep resistance than the DM one, especially at long term. The rather small improvement in the creep resistance due to the alumina content is likely linked with the fact that the initially high crystallinity of the POM was practically not influenced by the additives (PU and alumina). The results suggest further that the resistance to creep of the ternary systems is mostly governed by the PU phase.

Tensile tests

The effects of PU and alumina on the tensile mechanical data of POM systems are displayed in Figure 12. Addition of PU to POM or the combined use of PU and alumina improves the elongation at break, however, at cost of the tensile strength. The POM/PU/alumina ternary composites prepared by the MB method exhibited higher tensile strength accompanied by much higher elongation at break when compared with the composite produced by DM or to the POM/PU blend. Recall that the alumina particles are by far better dispersed in the matrix when prepared via the MB instead of the DM technique (cf. Figs. 2 and 3). This is in line with recent reports claiming that the tensile mechanical response is strongly affected by the dispersion state of nanofillers (e.g., Refs. 11 and 22). It is worth noting that increased ductility (elongation at break) generally manifests in improved toughness.

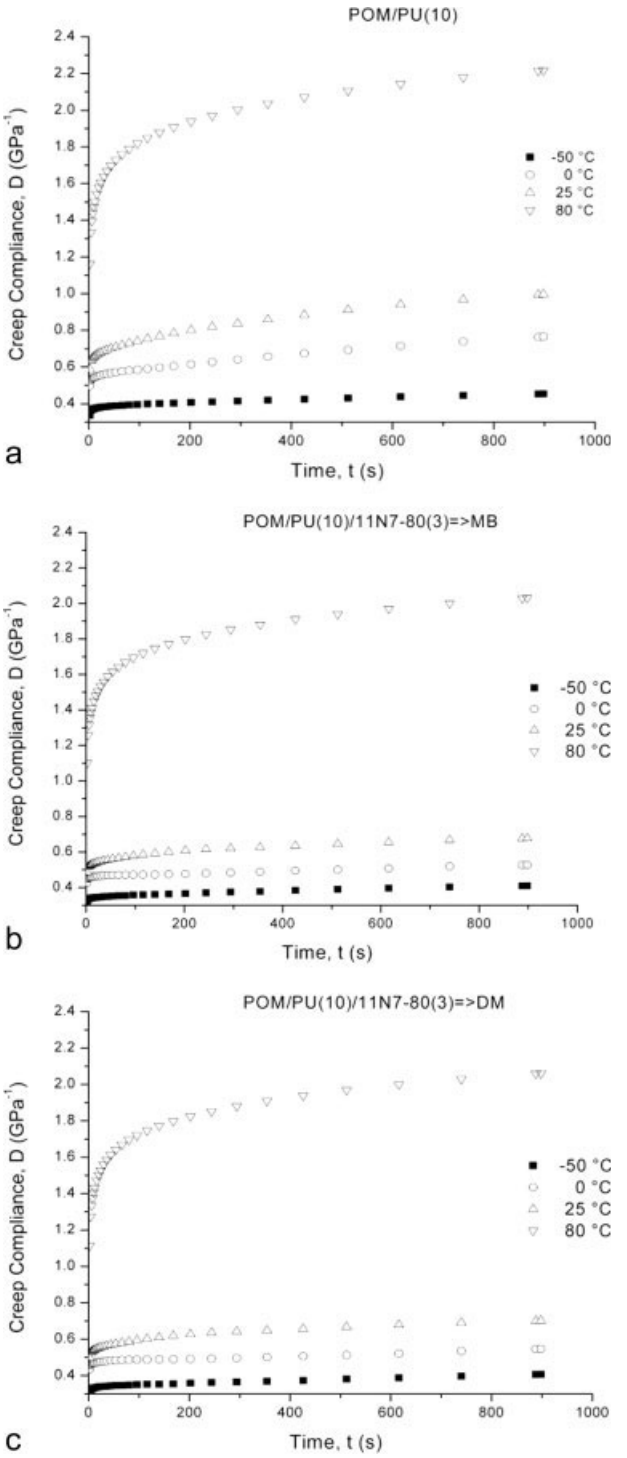

Figure 9 Effect of temperature on the tensile creep of (a) POM/PU blend, and for the ternary composites produced by (b) MB and (c) DM. For designation, cf. Figure 5.

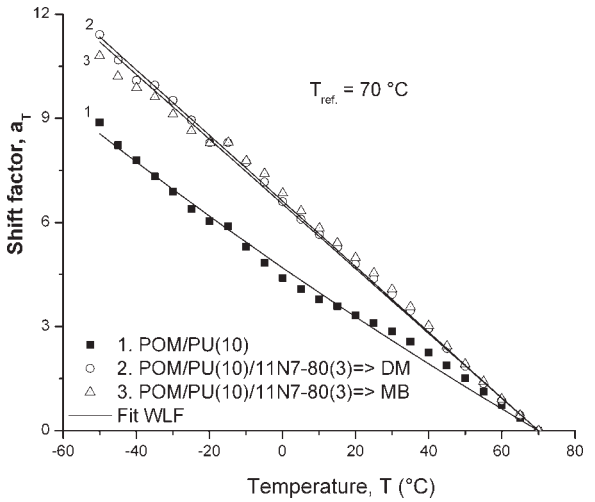

Figure 10 Experimental shift factors (logarithmic) of the systems studied along with the related WLF fits for the temperature range $T = -50$–80°C. For designation, cf. Figure 5.

Dielectric response

Figure 13 presents the dependence of the dielectric permittivity (ε′) and dissipation factor (tan δ) on the frequency, measured at RT for all the examined specimens. The dielectric permittivity and dissipation factor attain high values at the low frequency edge, which are decreasing steeply with increasing frequency. Considering the insulating nature of the examined systems, the enhanced values in the low frequency range indicate the coexistence of electrode polarization and interfacial relaxation phenomena. Electrode polarization is an undesirable effect related to the charged electrode-specimen contacts. Interfacial polarization (IP) or Maxwell-Wagner-Sillars (MWS) effects are present in heterogeneous systems

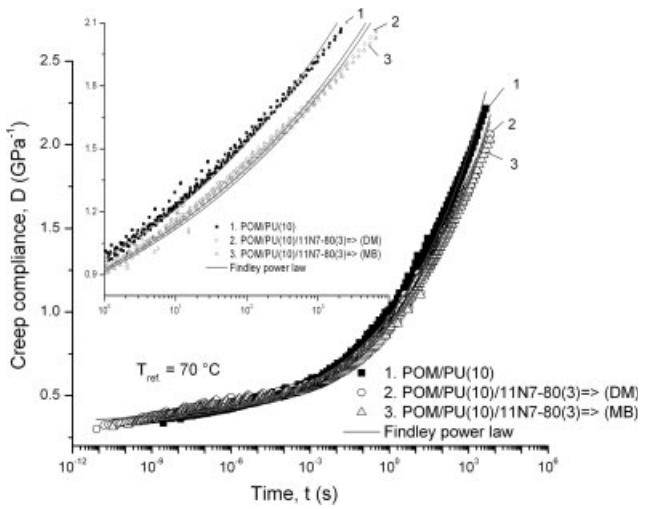

Figure 11 Creep master curves (compliance versus time) constructed by considering $T_0 = 70$°C and the related fits based on the Findley prediction. For designation, cf. Figure 5.

TABLE III
Findley Parameters for the Creep Master Curves of the POM-Based Systems Studied

Sample designation	D_{F0}	D_{F1}	n
POM/PU (10)	0.308	0.667	0.131
POM/PU (10)/11N7-80 (3) => (DM)	0.336	0.590	0.129
POM/PU (10)/11N7-80 (3) => (MB)	0.332	0.583	0.128

because of the accumulation of mobile charges at the interfaces of the composite.[23–26] Separating the contribution of each effect is not an easy procedure in the dielectric permittivity mode, and thus the electric modulus formalism will be used for the interpretation of dielectric data.

Electric modulus is defined as the inverse quantity of complex permittivity by the following equation:

$$M^* = \frac{1}{\varepsilon^*} = \frac{1}{\varepsilon' - j\varepsilon''} = \frac{\varepsilon'}{\varepsilon'^2 + \varepsilon''^2} + j\frac{\varepsilon''}{\varepsilon'^2 + \varepsilon''^2} = M' + jM'' \quad (5)$$

where ε′ and M' are the real, and ε″, M'' the imaginary parts of dielectric permittivity and electric modulus, respectively. Electric modulus presentation offers some advantages in the interpretation of bulk relaxation processes in complex systems, because the large variation in the permittivity and loss at low frequencies is minimized and difficulties occurring from the electrode-specimen contact due to the injection of space charges and absorbed impurities can be neglected.[27,28] The electric modulus formalism has been successfully used for the description of electrical relaxation phenomena in both micro and nanocomposites (e.g., Ref. 28).

Figure 14(a,b) depicts the real and imaginary parts of electric modulus (M', M'') as a function of

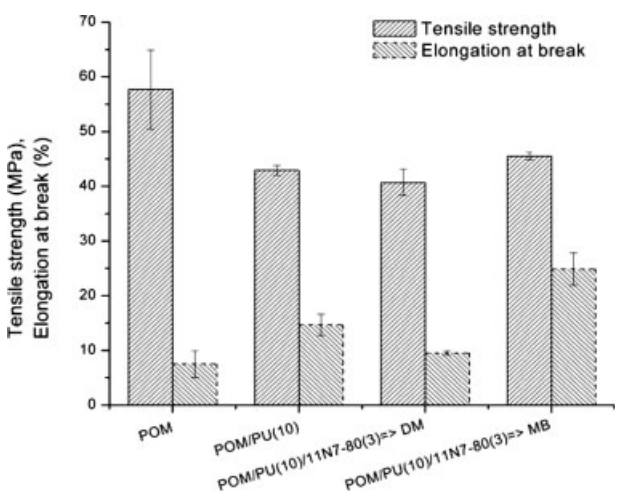

Figure 12 Tensile mechanical characteristics of the systems studied. For designation, cf. Figure 5.

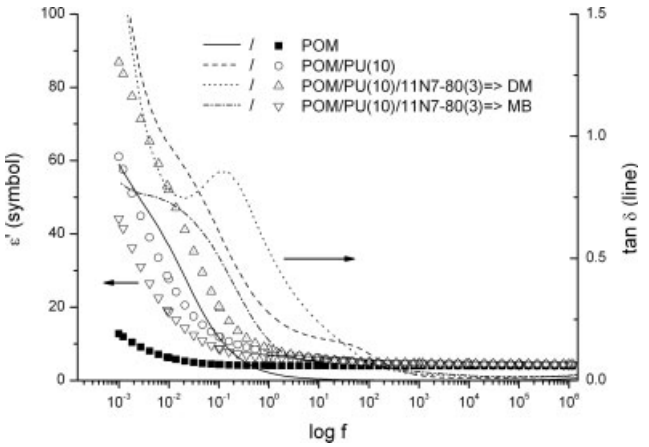

Figure 13 ε′ (separate symbols) versus frequency (*f*) and tan δ (line functions) versus f traces for the systems studied.

frequency for POM, POM/PU blend, and the composites produced by various methods. The real part of electric modulus (*M*′) as a function of frequency undergoes a steplike transition from low to high values for POM. On the other hand, the POM/PU blend and the MB and DM composites exhibit two-step-like transitions. These transitions imply the presence of relaxation processes. They become evident as loss peaks in the corresponding *M*″ versus frequency curves. In the dielectric spectrum (*M*″ versus frequency) of pure POM a single peak is recorded, assigned as α-relaxation [cf. Fig. 14(b)]. In the dielectric spectrum of POM, three transitions are expected to occur in accordance with the DMA results. However, only the slower transition is recorded in the examined frequency range at ambient temperature. Secondary modes (β and γ-relaxations) are characterized by relatively lower relaxation times, and thus they should be detected at lower temperatures (in isochronal scans) or higher frequencies (in isothermal scans).[29,30] The recorded α-relaxation process is often attributed to rearrangements in the crystalline parts of POM, although contributions from the amorphous phase cannot be excluded.[29,31] PU has a peak at 100 Hz (not shown here), related to its glass/rubber transition, and tends to form a second one at the high frequency edge, which is assigned to the reorientation of polar side groups of the main chain.[32,33] The dielectric spectra of the nanocomposites and the blend include the contributions of both polymers. It has to be mentioned that an analogous dielectric behavior has already been reported for PU-based systems containing alumina nanoparticles.[32] Moreover, the peak of neat POM (α-relaxation), recorded in the vicinity of 0.01 Hz, seems to shift toward higher frequencies in all other systems [cf. Fig. 14(b)]. By contrast, no such behavior is evident in the DMA results (cf. Fig. 6). Differences between the dielectric and the

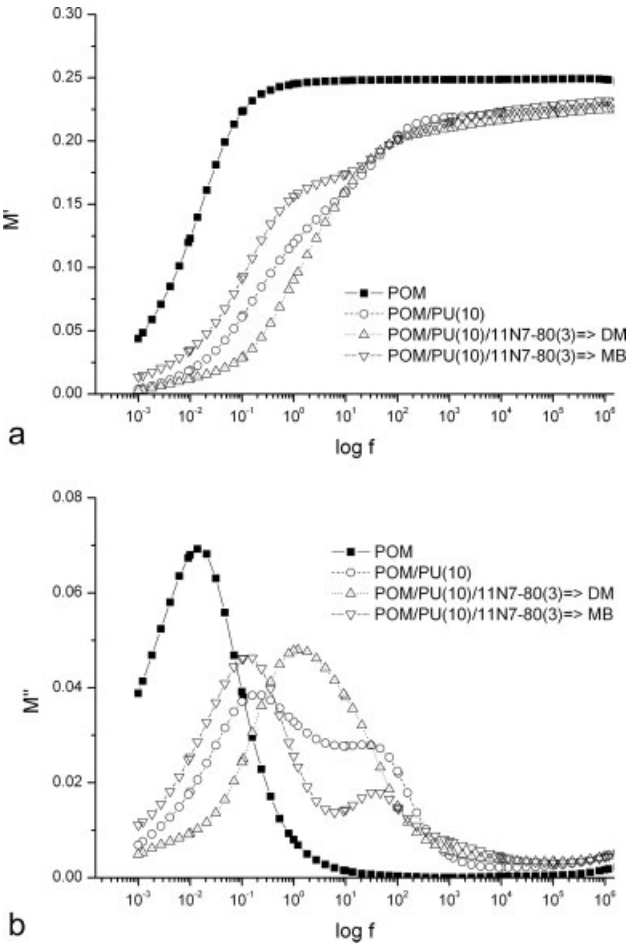

Figure 14 (a) Real (*M*′) and (b) imaginary part (*M*″) versus frequency traces for the POM, POM/PU blends, and POM/PU/alumina composites produced by various methods. For designation, cf. Figure 5.

DMA traces in crystalline polymers have been reported previously.[29,31] Finally, in the loss spectra of the complex systems, a small hump can be recognized in the low frequency edge, occurring from IP.

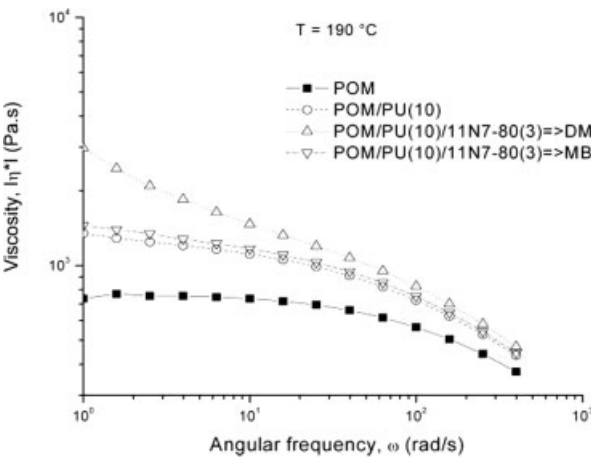

Figure 15 Melt viscosity versus angular frequency of the systems studied at $T = 190°C$. For designation, cf. Figure 5.

Melt rheology

The shear viscosity of POM, POM/PU blend, and POM/PU/alumina produced by MB and DM is shown in Figure 15. POM shows the presence of a linear viscoelastic region in the viscosity versus angular frequency curve. The shape of the viscosity curves of the composites prepared by MB is very similar to that of the POM/PU blend. On the other hand, the viscosity values of the composites produced by DM are always higher than those prepared by MB, albeit the difference is relatively high only at low angular frequencies. This is attributed to the large difference in the alumina dispersion between the composites produced by DM and MB, respectively. In the DM microcomposite, the alumina particles are separated from the PU phase and coarsely dispersed in the POM [cf. Fig. 3(b)]. On the other hand, the alumina particles are likely also dispersed in the PU phase in the MB nanocomposite. This assumption is in line with the rheological results in Figure 15, which were found reproducible.

CONCLUSION

Based on this work devoted to study, the potential benefits of PU latex-mediated dispersion of the alumina particles in ternary POM/PU/alumina composites produced by the MB and DM mixing, respectively, on the mechanical, thermal, and dielectrical properties, the following conclusions can be drawn:

- The dispersion of the alumina was markedly better when produced by MB compared to DM. Introduction of PU and alumina did not affect practically the crystallinity of the POM. The thermooxidative stability of the PU-toughened POM was markedly improved by the alumina particles present.
- Incorporation of PU decreased the stiffness (enhanced the compliance) of the related POM/PU blend that could be only partly compensated by the alumina filler.
- The preparation techniques of the composites (MB and DM) had a strong effect on the tensile mechanical, dielectric, and rheological properties. On the other hand, the preparation method marginally influenced the TGA and creep responses. The creep behavior was suggested to be controlled by the PU phase along with its dispersion.

S. Siengchin thanks the DFG (German Science Foundation) for the fellowship in the framework of the graduate school GRK 814. The authors are thankful to Dr. N. Papke (Ticona, Frankfurt, Germany) for providing the POM material.

References

1. Plummer, C. J G.; Scaramuzzino, P.; Kausch, H.-H.; Philippoz, J.-M. Polym Eng Sci 2000, 40, 1306.
2. Sukhanova, T.; Bershtein, V.; Keating, M.; Matveeva, G.; Vylegzhanina, M.; Egorov, V.; Peschanskaya, N.; Yakushev, P.; Flexman, E.; Greulich, S.; Sauer, B.; Schodt, K. Macromol Symp 2004, 214, 135.
3. Lesser, A. J Polym Eng Sci 1996, 36, 2366.
4. Plummer, C. J. G.; Menu, P.; Cudré-Mauroux, N.; Kausch, H.-H. J Appl Polym Sci 1995, 55, 489.
5. Xu, W.; He, P. J Appl Polym Sci 2001, 80, 304.
6. Mehrabzadeh, M.; Rezaie, D. J Appl Polym Sci 2002, 84, 2573.
7. Chiang, W.-Y.; Lo, M.-S. J Appl Polym Sci 1988, 36, 1685.
8. Kawaguchi, K.; Tajima, Y. J Appl Polym Sci 2006, 100, 4375.
9. Gao, X.; Qu, C.; Zhang, Q.; Peng, Y.; Fu, Q. Polym Int 2004, 53, 1666.
10. Gao, X.; Qu, C.; Zhang, Q.; Peng, Y.; Fu, Q. Macromol Mater Eng 2004, 289, 41.
11. Karger-Kocsis, J.; Zhang, Z. In Mechanical Properties of Polymers Based on Nanostructure and Morphology; Michler, G. H., Baltá-Calleja, F. J., Eds.; CRC Press: Boca Raton, FL, 2005; Chapter 13, pp 553–602.
12. Siengchin, S.; Karger-Kocsis J. Macromol Rapid Commun 2006, 27, 2090.
13. Siengchin, S.; Karger-Kocsis, J.; Thomann, R. J Appl Polym Sci 2007, 105, 2963.
14. Wang, Y.; Li, Y.; Zhang, R.; Huang, L.; He, W. Polym Compos 2006, 27, 282.
15. Horrion, J.; Cartasegna, S.; Agarwal, P. K. Polym Eng Sci 1996, 36, 2061.
16. Sun, T. J.; Ye, L.; Zhao, X. W. Plast Rubber Compos 2007, 36, 350.
17. Kaito, A.; Nakayama, K.; Kanetsuna, H. J Appl Polym Sci 1986, 32, 3499.
18. Hojfors, R. J.; Baer, E.; Geil, P. H. J. Macromol Sci Phys 1977, B13, 323.
19. Ferry, J. D. Viscoelastic Properties of Polymers; Wiley: New York, 1980.
20. Findley, W. N.; Lai, J. S.; Onaran, K. Creep and Relaxation of Nonlinear Viscoelastic Materials; Dover: New York, 1989.
21. Yang, J. L.; Zhang, Z.; Schlarb, A. K.; Friedrich, K. Polymer 2006, 47, 6745.
22. Siengchin, S.; Karger-Kocsis, J.; Apostolov, A. A.; Thomann, R. J Appl Polym Sci 2007, 106, 248.
23. Van Beck, L. K. H. In Progress in Dielectrics; Briks, J. B., Ed.; Heywood Books: London, 1967; pp 69–117.
24. Sillars, R. W. J Inst Elect Eng 1937, 80, 378.
25. Hedvig, P. Dielectric Spectroscopy of Polymers; Adam Hilger: Bristol, 1977; p 283.
26. Tsangaris, G. M.; Psarras, G. C. J Mater Sci 1999, 34, 2151.
27. Tsangaris, G. M.; Psarras, G. C.; Kouloumbi, N. J Mater Sci 1998, 33, 2027.
28. Psarras, G. C.; Gatos, K. G.; Karahaliou, P. K.; Georga, S. N.; Krontiras, C. A.; Karger-Kocsis, J. Expr Polym Lett 2007, 1, 837.
29. Sauer, B. B.; Avakian, P.; Flexman, E. A.; Keating, M.; Hsiao, B. S.; Verma, R. K. J Polym Sci Part B: Polym Phys 1997, 35, 2121.
30. Wasylyshyn, D. A. IEEE Trans Dielectr Electr Insul 2005, 12, 183.
31. Boyd, R. H. Polymer 1985, 26, 1123.
32. Gatos, K. G.; Alcázar, J. G. M.; Psarras, G. C.; Thomann, R.; Karger-Kocsis, J. Compos Sci Technol 2007, 67, 157.
33. Psarras, G. C.; Gatos, K. G.; Karger-Kocsis, J. J Appl Polym Sci 2007, 106, 1405.